De novo mutations of the ATP6V1A gene cause developmental encephalopathy with epilepsy

Anna Fassio,[1,2,*] Alessandro Esposito,[1,2,*] Mitsuhiro Kato,[3] Hirotomo Saitsu,[4] Davide Mei,[5] Carla Marini,[5] Valerio Conti,[5] Mitsuko Nakashima,[4,6] Nobuhiko Okamoto,[7] Akgun Olmez Turker,[8] Burcu Albuz,[9] C. Nur Semerci Gündüz,[9] Keiko Yanagihara,[10] Elisa Belmonte,[1] Luca Maragliano,[2] Keri Ramsey,[11] Chris Balak,[11] Ashley Siniard,[11] Vinodh Narayanan,[11] C4RCD Research Group,[11] Chihiro Ohba,[6] Masaaki Shiina,[12] Kazuhiro Ogata,[12] Naomichi Matsumoto,[6] Fabio Benfenati[1,2] and Renzo Guerrini[5,13]

*These authors contributed equally to this work.

V-type proton (H⁺) ATPase (v-ATPase) is a multi-subunit proton pump that regulates pH homeostasis in all eukaryotic cells; in neurons, v-ATPase plays additional and unique roles in synapse function. Through whole exome sequencing, we identified *de novo* heterozygous mutations (p.Pro27Arg, p.Asp100Tyr, p.Asp349Asn, p.Asp371Gly) in *ATP6V1A*, encoding the A subunit of v-ATPase, in four patients with developmental encephalopathy with epilepsy. Early manifestations, observed in all patients, were developmental delay and febrile seizures, evolving to encephalopathy with profound delay, hypotonic/dyskinetic quadriparesis and intractable multiple seizure types in two patients (p.Pro27Arg, p.Asp100Tyr), and to moderate delay with milder epilepsy in the other two (p.Asp349Asn, p.Asp371Gly). Modelling performed on the available prokaryotic and eukaryotic structures of v-ATPase predicted p.Pro27Arg to perturb subunit interaction, p.Asp100Tyr to cause steric hindrance and destabilize protein folding, p.Asp349Asn to affect the catalytic function and p.Asp371Gly to impair the rotation process, necessary for proton transport. We addressed the impact of p.Asp349Asn and p.Asp100Tyr mutations on ATP6V1A expression and function by analysing ATP6V1A-overexpressing HEK293T cells and patients' lymphoblasts. The p.Asp100Tyr mutant was characterized by reduced expression due to increased degradation. Conversely, no decrease in expression and clearance was observed for p.Asp349Asn. In HEK293T cells overexpressing either pathogenic or control variants, p.Asp349Asn significantly increased LysoTracker® fluorescence with no effects on EEA1 and LAMP1 expression. Conversely, p.Asp100Tyr decreased both LysoTracker® fluorescence and LAMP1 levels, leaving EEA1 expression unaffected. Both mutations decreased v-ATPase recruitment to autophagosomes, with no major impact on autophagy. Experiments performed on patients' lymphoblasts using the LysoSensor™ probe revealed lower pH of endocytic organelles for p.Asp349Asn and a reduced expression of LAMP1 with no effect on the pH for p.Asp100Tyr. These data demonstrate gain of function for p.Asp349Asn characterized by an increased proton pumping in intracellular organelles, and loss of function for p.Asp100Tyr with decreased expression of ATP6V1A and reduced levels of lysosomal markers. We expressed p.Asp349Asn and p.Asp100Tyr in rat hippocampal neurons and confirmed significant and opposite effects in lysosomal labelling. However, both mutations caused a similar defect in neurite elongation accompanied by loss of excitatory inputs, revealing that altered lysosomal homeostasis markedly affects neurite development and synaptic connectivity. This study provides evidence that *de novo* heterozygous *ATP6V1A* mutations cause a developmental encephalopathy with a pathomechanism that involves perturbations of lysosomal homeostasis and neuronal connectivity, uncovering a novel role for v-ATPase in neuronal development.

1 Department of Experimental Medicine, University of Genoa, Genoa, Italy
2 Center of Synaptic Neuroscience and Technology, Istituto Italiano di Tecnologia, Genoa, Italy
3 Department of Paediatrics, Showa University School of Medicine, Tokyo, Japan

4　Department of Biochemistry, Hamamatsu University School of Medicine, Hamamatsu, Japan
5　Pediatric Neurology, Neurogenetics and Neurobiology Unit and Laboratories, Children's Hospital A. Meyer-University of Florence, Florence, Italy
6　Department of Human Genetics, Yokohama City University Graduate School of Medicine, Yokohama, Japan
7　Department of Medical Genetics, Osaka Women's and Children's Hospital, Osaka, Japan
8　Private Clinic, Denizli, Turkey
9　Department of Medical Genetics, Pamukkale University Hospital, Denizli, Turkey
10　Department of Paediatric Neurology, Osaka Women's and Children's Hospital, Osaka, Japan
11　Center for Rare Childhood Disorders and Neurogenomics Division Translational Genomics Research Institute, Phoenix, Arizona 85004, USA
12　Department of Biochemistry, Yokohama City University Graduate School of Medicine, Yokohama, Japan
13　IRCCS Fondazione Stella Maris, Pisa, Italy

Correspondence to: Prof. Renzo Guerrini
Neuroscience Department, Anna Meyer Children's University Hospital, Florence Italy
E-mail: r.guerrini@meyer.it

Correspondence may also be addressed to: Prof. Anna Fassio
Department of Experimental Medicine, University of Genoa, Italy
E-mail: afassio@unige.it

Prof. Naomichi Matsumoto
Department of Human Genetics, Yokohama City University, Japan
E-mail: naomat@yokohama-cu.ac.jp

Introduction

V-type proton (H$^+$) ATPase (v-ATPase) is a multimeric complex that acts as an ATP-dependent proton pump. V-ATPase is composed of a peripheral V_1 domain that hydrolyses ATP and an integral V_0 domain that translocates protons by a rotary mechanism. V-ATPase is responsible for membrane trafficking processes such as receptor-mediated endocytosis, intracellular trafficking of lysosomal enzymes, and acidification of intracellular organelles in all eukaryotic cells (Forgac, 2007; Cotter *et al.*, 2015). Despite the ubiquitous role in pH homeostasis and intracellular signalling pathways, the v-ATPase complex is expressed at high levels in neurons where it plays additional and unique roles in neurotransmitter loading into synaptic vesicles and in regulating synaptic transmission (Morel and Poëa-Guyon, 2015; Bodzęta *et al.*, 2017).

In humans, a redundant set of subunits is encoded by 22 autosomal genes, allowing the composition of diverse v-ATPase complexes with specific properties and tissue expression. Among these, seven have been associated with human disease (Supplementary Table 1). Six subunits have been related to recessive disorders, including distal renal tubular acidosis and hearing loss (ATP6V1B1 and ATP6V0A4) (Karet *et al.*, 1999; Smith *et al.*, 2000; Stover *et al.*, 2002), osteopetrosis with macrocephaly, progressive deafness, blindness, hepatosplenomegaly, and severe anaemia (ATP6V0A3) (Frattini *et al.*, 2000; Kornak *et al.*, 2000), and cutis laxa, a systemic disease with severe neurological impairment featuring structural brain abnormalities, profound delay, and seizures (ATP6V0A2, ATP6V1E1 and ATP6V1A) (Kornak *et al.*, 2008; Fischer *et al.*, 2012; Van Damme *et al.*, 2017). Two allelic dominant disorders, Zimmermann-Laband syndrome type 2, featuring facial dysmorphisms and intellectual disability (Kortum *et al.*, 2015) and a form of congenital deafness with anonyochia, have also been described (ATP6V1B2) (Yuan *et al.*, 2014).

Through whole exome sequencing of 1444 patients with developmental encephalopathies and epilepsy, we identified in four patients heterozygous *de novo* missense mutations in *ATP6V1A* (p.Pro27Arg, p.Asp100Tyr, p.Asp349Asn, p.Asp371Gly), all involving highly evolutionarily conserved residues in functionally relevant regions of the molecule. Functional analysis conducted for the p.Asp100Tyr and p.Asp349Asn mutations demonstrated a loss-of-function mechanism involving increased ATPase degradation and lysosomal defects for the former, and a gain-of-function mechanism consisting of increased acidification of intracellular organelles for the latter. In neurons, both ATP6V1A mutants caused a defect in neurite elongation, accompanied by a significant loss of excitatory synapses, suggesting a crucial and unexplored role of v-ATPase in neuronal development and synapse formation. We provide evidence that *de novo* heterozygous *ATP6V1A* mutations cause a developmental encephalopathy with epilepsy with a pathomechanism that involves the effects of v-ATPase in lysosomal homeostasis and neuronal connectivity. This study also demonstrates that *ATP6V1A* mutations can be disease causing at the heterozygous state, although previously described biallelic phenotypes are more severe.

Patients and methods

Patients

Exome studies were conducted in three cohorts, including patients of different ethnicities (Supplementary Table 2A), with developmental delay/intellectual disability and epilepsy of presumed genetic origin. The overall series consisted of 1444 probands, most of whom were part of a trios study. Patients were assigned to eight specific epileptic encephalopathy syndromes, plus a ninth subgroup of 'unclassified' epileptic encephalopathies with mixed seizure disorders that could not be assigned to a specific syndrome (Supplementary Table 2B). All four patients with *ATP6V1A* mutations belonged to the latter subgroup.

All participants to the study had signed an informed consent for research whole exome sequencing studies. The study was approved by the Paediatric Ethic Committee of the Tuscany Region, in the context of the DESIRE project (Seventh Framework Programme FP7; grant agreement n° 602 531).

Whole exome sequencing

In 900 patients, whole exome sequencing was performed with the SureSelectXT Human All Exon v5 or v6 (Agilent Technologies). Captured libraries were sequenced using Illumina Hiseq 2500 (Illumina) with 101-base paired-end reads. Exome data processing, variant calling, and variant annotation were performed as previously described (Saitsu *et al.*, 2013). In singleton probands exhibiting *de novo* mutations, parentage was confirmed by microsatellite analysis, as previously described (Saitsu *et al.*, 2013). In 494 patients, whole exome sequencing was performed and analysed as previously described (Narayanan *et al.*, 2015). In 50 additional patients, exons were captured from fragmented genomic DNA samples using the SureSelect Human All Exon v4 (Agilent Technologies), and paired-end 90-base massively parallel sequencing was carried out on an Illumina HiSeq 2000, according to the manufacturer's protocols (Illumina). In the latter group, bioinformatics analysis was carried out using an in-house developed pipeline. Sequencing reads passing quality filtering were aligned to the human reference genome (hg19) with Burrows-Wheeler Aligner (BWA) (Li and Durbin, 2010). The Genome Analysis Toolkit (GATK) (McKenna *et al.*, 2010) was used for base quality score recalibration, indel realignment, duplicate removal, and to perform SNP and INDEL discovery and genotyping across all samples simultaneously using variant quality score recalibration according to GATK Best Practices recommendations (DePristo *et al.*, 2011; Van der Auwera *et al.*, 2013). For annotating and filtering data, the SNPeff program was used (Cingolani *et al.*, 2012). The *de novo* variants were called using the DeNovoGear tool with a 0.8 threshold at the posterior probability of the most likely *de novo* genotype configuration (Ramu *et al.*, 2013). All samples had a mean depth of target region covered at 112× and >97% of bases in the consensus coding sequences covered by at least 20 reads. We excluded variants with minor allele frequency (MAF) >1% in either the 1000 Genomes Project (1000g) or the Exome Aggregation Consortium (ExAC v0.3) databases.

In patients carrying *ATP6V1A* variants, we excluded *de novo* or recessive (MAF < 1%) variants in the well-established genes for epileptic encephalopathies (listed in Supplementary Table 3) and submitted for validation and segregation testing by Sanger sequencing of candidate *de novo* variants that were predicted to alter protein function (non-synonymous, stop-gain, stop-loss, frameshift, and splice-junction mutations).

We evaluated whether the *ATP6V1A* human protein-coding gene is likely to harbour disease-causing mutations using different gene-level prediction tools including the ExAC (Exome Aggregation Consortium) constraint metrics (Lek *et al.*, 2016), the residual variation intolerance score (RVIS; based on ExAC v2 release 2.0) (Petrovski *et al.*, 2013) and the gene damage index (GDI) (Itan *et al.*, 2015). Furthermore, to improve the use of existing variant-level methods such as the Combined Annotation Dependent Depletion (CADD) score (Kircher *et al.*, 2014) and test the four missense substitutions we identified in *ATP6V1A*, we also used the mutation significance cut-off (MSC) server (Itan *et al.*, 2016), a quantitative approach that provides gene-level and gene-specific phenotypic impact cut-off values.

We evaluated mutations' pathogenicity for the four *ATP6V1A* variants through *in silico* prediction using the dbNSFP database (v3.0a), which provides functional prediction scores on more than 20 different algorithms (https://sites.google.com/site/jpopgen/dbNSFP). To assess the effects of the four missense *ATP6V1A* substitutions, we used both the dbNSFP ensemble rank scores MetaSVM and MetaLR (Liu *et al.*, 2016). In addition, we used the scores obtained from Revel (Ioannidis *et al.*, 2016), M-CAP (Jagadeesh *et al.*, 2016) and Eigen (Ionita-Laza *et al.*, 2016), three different bioinformatics tools to evaluate the pathogenicity of rare variants.

We performed conservation analysis across species (orthologous sequences) using a multiple sequence alignment (MSA) of the ATP6V1A protein sequence. The MSA (MUSCLE algorithm) and the sequence logo consensus were generated by the Jalview software (http://www.jalview.org). Residues were coloured according to their physicochemical properties (Zappo colour scheme).

To evaluate if *de novo ATP6V1A* variants had ever been reported, either in affected individuals or controls, we interrogated the denovo-db database (Turner *et al.*, 2017).

ATP6V1A gene *de novo* mutation enrichment analysis

To assess whether in the 1444 probands cohort the *ATP6V1A* gene was enriched in missense *de novo* mutations, we used the freely available R package DenovolyzeR (Ware *et al.*, 2015) and gene-specific mutation rates originally reported by Samocha *et al.* (2014). The *ATP6V1A de novo* gene-specific *P*-value calculated by DenovolyzeR for missense variants was corrected for multiple testing (Bonferroni correction), according to the 19 618 genes for which mutation rates are available, and the number of tests (one test for the missense class). The genome-wide Bonferroni corrected *P*-value threshold at $\alpha = 0.05$ for one test was 2.55×10^{-6} [0.05/(1 × 19 168)]. We carried out the *ATP6V1A de novo* mutation enrichment analysis in the overall cohort without any stratification using the RStudio software (rstudio.com).

To rule out that the four variants could have arisen by chance, we performed the chi-squared test with Yates correction for a 2×2 contingency table (patients carrying the variants/mutation negative patients versus controls carrying the variants/mutation negative controls) using the QuickCalcs tool (graphpad.com/quickcalcs/contingency1.cfm). For each variant, we carried out the test on exome data of our cohort and the Genome Aggregation Database (gnomAD) cohorts, both at large and through ethnicity-matched analysis.

Structural modelling

We searched the crystal structure homologous to human ATP6V1A using the protein homology/analogy recognition engine, Phyre2 (Kelley *et al.*, 2015). We calculated the free energy change upon the Asp85Tyr mutation with the FoldX software (foldxsuite.crg.eu) using the crystal structure of the V_1 domain from *Enterococcus hirae* v-ATPase in a nucleotide-bound state (PDB code 3VR6). The molecular structures were drawn using PyMOL (Schrödinger, New York, NY). Using the same Phyre2 server, we also obtained the alignment of human ATP6V1A and *Saccharomyces cerevisiae* A subunit primary sequences. The homology model was created using I-TASSER (Roy *et al.*, 2010), with the A subunit of *S. cerevisiae* v-ATPase (PDB code 3J9T) as template.

ATP6V1A constructs

We synthesized wild-type and mutant (p.Asp100Tyr and p.Asp349Asn) human *ATP6V1A* cDNAs *in vitro* and cloned in pLVX-IRES-mCherry vector by Biomatik. We performed Sanger sequencing of all constructs to check the correct inserts orientation and validate their sequence.

Cell culture and transfection

Human embryonic kidney-derived 293T (HEK) cells were maintained at 37°C in a humidified 5% CO_2 incubator in DMEM (Life Technologies) supplemented with 10% FBS, 2 mM L-glutamine and 1% Penicillin-Streptomycin. Cells were transfected with Lipofectamine 2000 (Life Technologies) according to the manufacturer's instructions. HEK cells were starved by medium withdrawal for 2 h. Lymphoblatsts were prepared by infecting lymphocytes obtained from patients and their parents with the Epstein-Barr virus (EBV) *in vitro* using standard protocols and maintained in RPMI 20% foetal bovine serum (FBS), 1 mM L-glutamine and 10 mM D-glucose. Primary cortical neurons were prepared from embryonic Day 18 brains of Sprague Dawley rats as previously described (Verstegen *et al.*, 2014). Neurons were transfected using Lipofectamine® 2000 at 7 or 14 days *in vitro* (DIV) and analysed 3 days after transfection.

Western blotting

Protein lysates from HEK, lymphoblast and neuronal cultures were extracted in lysis buffer [50 mM Tris (pH 7.5), 150 mM NaCl, 0.1% SDS, 1% Nonidet P40, 0.2 mM phenylmethylsulfonyl fluoride, 2 µg/ml pepstatin, and 1 µg/ml leupeptin] and then separated by SDS-PAGE and assayed by immunoblotting with the following primary antibodies: anti-ATP6V1A (1:1000; #ab137574, Abcam), anti-ATP6V1B2 (1:2000; #ab73404, Abcam), anti-LAMP1 (1:1000; #ab24170, Abcam), anti-EEA1 (1:5000; #610457, BD Bioscience), LC3B (1:1000; #7543, Sigma-Aldrich), p62 (1:1000, #P0067, Sigma-Aldrich), anti-GAPDH (1/1000; #SC-25778, Santa Cruz Biotechnology), anti-VAMP2 (1:1000; #104202; Synaptic Systems); anti-V-GLUT1 (1:1000; #135304, Synaptic Systems) anti-PSD95 (1:1000; #SC-32290, Santa Cruz Biotechnology).

Degradation assay

HEK cells were transfected with ATP6V1A wild-type, ATP6V1A Asp349Asn or ATP6V1A Asp100Tyr and treated with 10 µg/ml of cycloheximide (C4859, Sigma-Aldrich) 24 h after transfection. Cells were lysed at different times after cycloheximide addition and analysed by western blotting. Protein level is expressed with respect to ATP6V1A content in the cells collected at time zero and treated with vehicle (DMSO).

Immunocytochemistry and fluorescence microscopy

Transfected primary cortical neurons or HEK cells were fixed in 4% paraformaldehyde in phosphate-buffered saline (PBS), permeabilized in 0.1% Triton™ X-100, blocked with 2% FBS/0.05% Tween-20 in PBS and incubated with the various antibodies in blocking solution. Samples were mounted in ProLong® Gold antifade reagent with DAPI (#P36935, Thermo-Fisher Scientific). Capture of confocal images was performed using a laser scanning confocal microscope (SP5, Leica) with a $40\times$ or $63\times$ oil-immersion objective. For LAMP1 (1:200, #L1418 Sigma-Aldrich) and EEA1 (1:500; #610457, BD Bioscience), ATP6V1B2 (1:200, #SAB1405501 Sigma-Aldrich) and LC3B (1:200, #2775 Cell Signalling) labelling, each image consisted of a stack of images taken through the *z*-plane of the cell. The co-localization of ATP6V1B2 and LC3B signals was analysed using the ImageJ intensity correlation analysis plugin to calculate Pearson's correlation coefficient. For LysoTracker® Deep Red (Molecular Probes/Life Technologies) experiments, HEK cells were incubated with 200 nM LysoTracker® for 1 h, whereas neurons were incubated with 50 nM LysoTracker® for 30 min, at 37°C in culture medium, immediately fixed and analysed within 12 h. Images were taken at either epifluorescence (Olympus 1X81) or confocal (SP5, Leica) microscope in a single plane not to fade the fluorescent signal. Settings were kept the same for all acquisitions within each experiment.

Measurement of endo-lysosomal pH

Endo-lysosomal pH was measured using a ratiometric pH indicator dye, LysoSensor™ Yellow/Blue dextran (Molecular Probes/Life Technologies), a dual excitation dye that allows pH measurement in endocytic organelles independently of dye concentration. Lymphoblasts (4×10^6) were incubated for 3 h at 37°C with 0.5 mg/ml of LysoSensor™ Yellow/Blue dextran in culture medium. Cells were divided into five samples, four to perform the calibration curve and one for the measurements. To obtain a pH calibration curve, cells were resuspended with MES calibration buffer solution

(5 mM NaCl, 115 mM KCl, 1.2 mM MgSO$_4$ and 25 mM MES, pH ranging from 3.7 to 7.6) containing 10 μM monensin (Sigma-Aldrich) and 10 μM nigericin (Sigma-Aldrich). For the pH measures, cells were resuspended in MES calibration buffer solution pH 7.7 in the absence of ionophores. Emission scans were collected at 450 nm and 528 nm with the Luminescence Spectrometer LS 50 (Perkin Elmer), using excitation at 360 nm and emission/excitation bandwidths set to 4 nm. Calibration data (ratio 450/528) were fitted to a linear regression with the software GraphPad Prism5 and the sample ratios converted into absolute pH values by interpolation in the calibration function.

Sholl analysis

Neurons were plated at low density (80 cells/mm^2), transfected at 7 DIV and analysed at 10 DIV. For analysis, neurons were fixed in 4% PFA, in PBS and decorated with βIII tubulin antibody (1:1000, #MMS-435P Covance) followed by Alexa Fluor® 488 secondary antibody to unequivocally distinguish neuronal cells. The extent of neurite arborization was evaluated using Sholl analysis as previously described (Falace *et al.*, 2010). Concentric circles with radii increasing at regular 10-μm steps were centred to the cell body and the number of intersections was automatically evaluated with the ImageJ/Sholl analysis plug-in.

Synapse quantification

Neurons, plated at low density as described above, were either transfected at 14 DIV and analysed at 17 DIV or treated at 17 DIV with 200 nM leupeptin for 3 h (#EI8, MerckMillipore; Goo *et al.*, 2017). To measure excitatory synapses, neurons were labelled with anti-V-GLUT1 (1/500, #135304; Synaptic Systems) and anti-Homer1 (1/200, #160011; Synaptic Systems) antibodies. Confocal images were acquired with a laser scanning confocal microscope (SP5 Upright, Leica) with a 40× oil-immersion objective. Each image consisted of a stack of images taken through the *z*-plane of the cell. Confocal microscope settings were kept the same for all scans in each experiment. The co-localization analysis was performed by evaluating the labelling of the VGLUT1/Homer1 synaptic protein couples. Co-localization puncta with areas of 0.1–2 μm^2 were considered *bona fide* synaptic boutons. Synaptic boutons along Cherry-positive neurites were manually counted on 30 μm puncta starting from the cell body.

Results

Identification of *ATP6V1A* mutations

Trio-based whole exome sequencing studies revealed *de novo* mutations in *ATP6V1A* (MIM 607 027; RefSeq accession number NM_001690.3), encoding the ATPase H$^+$ transporting V$_1$ subunit A in three patients [Patient 1: c.298G > T (p.Asp100Tyr); Patient 2: c.1045G > A (p.Asp349Asn); and Patient 4: c.80C > G (p.Pro27Arg)]. A subsequent search for *ATP6V1A* variants in whole exome sequencing data obtained from singleton patients, identified an additional patient carrying a *de novo*
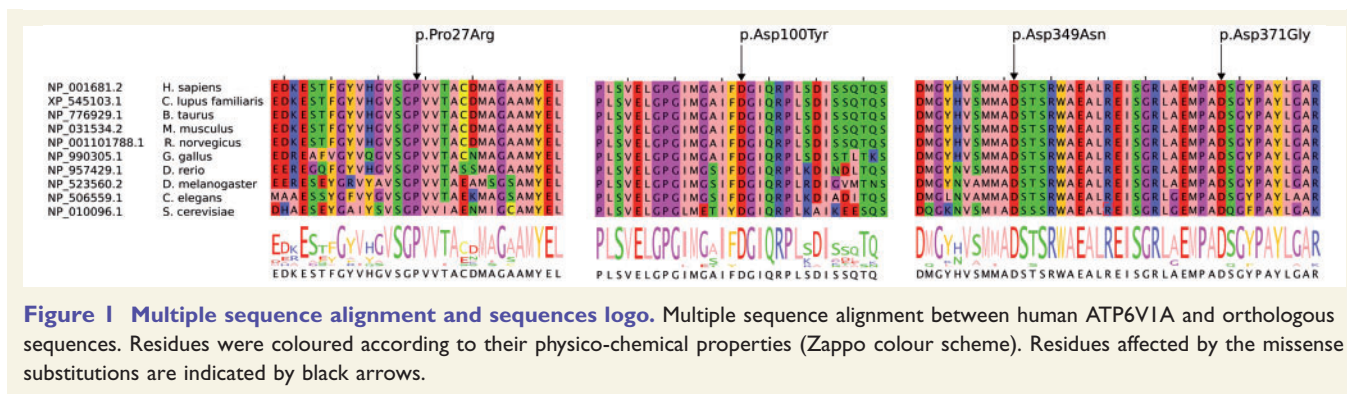
heterozygous *ATP6V1A* variant [Patient 3: c.1112A > G (p.Asp371Gly)]. Patients 1–3 were identified via an ongoing collaboration matching exome data generated in Europe by the DESIRE project on rare developmental/epileptic encephalopathies (http://epilepsydesireproject.eu) with those of a comparable cohort in Japan. Patient 4 was subsequently identified through DESIRE dissemination activities, after preliminary data on the first three patients were made available in the project website. We also screened for *ATP6V1A* inherited variants with a frequency <1% in the 1000 Genomes Project (1000g) or in the Exome Aggregation Consortium (ExAC) databases, both in cases of homozygous recessive or compound heterozygous state.

None of the *de novo* *ATP6V1A* identified mutations was observed in the 1000g, ExAC, gnomAD or dbSNP (build 147) databases. We confirmed the mutations and their *de novo* nature on genomic DNA of probands and parents by Sanger sequencing. Patient 3 parentage was confirmed using 12 microsatellite markers.

All four highly functionally relevant *de novo* mutations caused missense substitutions at evolutionarily conserved amino acid positions (Fig. 1) and were predicted to be damaging by *in silico* methods (Supplementary Table 4A). ExAC constraint metrics indicated that *ATP6V1A* has fewer variants than expected and is intolerant both to loss-of-function (pLI = 0.99) and missense variants (Z-score = 3.03). The RVIS (RVIS score −0.7; RVIS percentile 20.93%) and the GDI (GDI score 22.7; GDI_Phred 0.76) scores also highlight *ATP6V1A* intolerance to variations. Finally, the MSC damage prediction (99% confidence interval) tool highlights the highly damaging impact the p.Pro27Arg, p.Asp100Tyr, p.Asp349Asn, and p.Asp371Gly substitutions have on the ATP6V1A protein, according to the MSC CADD corrected scores (Supplementary Table 4B).

To explore pathogenicity of the four variants further, we performed gene-specific *de novo* mutation enrichment analysis and a variant-specific chi-squared test with Yates correction for a 2 × 2 contingency table. The *ATP6V1A* missense *de novo* mutations enrichment analysis performed with DenovolyzeR (*n* = 1444, *de novo* mutations observed = 4, *de novo* mutations expected = 0.1, enrichment 79) reached genome-wide statistical significance (P-value of 2.63 × 10^{-7}; Bonferroni correct threshold P-value 2.55 × 10^{-6}). All four variants reached significant values (P < 0.0001) in the chi-squared test performed using the 123 136 gnomAD exomes as control (Supplementary Table 5A). Performing the same analysis matching the four mutations versus ethnically matched subpopulations, all mutations maintained significant values (Supplementary Table 5B–E). These data suggest that the *ATP6V1A* mutations did not occur by chance in the cohort studied.

The denovo-db returned only five *de novo* hits (three intronic and two missense substitutions) in *ATP6V1A*. The two missense substitutions were p.Asp11Asn, identified in a male with autism spectrum disorder (Iossifov *et al.*, 2014), and p.Pro249Arg identified in another male with a

Figure 1 Multiple sequence alignment and sequences logo. Multiple sequence alignment between human ATP6V1A and orthologous sequences. Residues were coloured according to their physico-chemical properties (Zappo colour scheme). Residues affected by the missense substitutions are indicated by black arrows.

severe developmental disorder (McRae *et al.*, 2017). These two missense substitutions, however, have not been subjected to orthogonal validation and should therefore be considered as 'potential' *de novo* variants. These data further highlight how rare *de novo* mutations are in the *ATP6V1A* gene.

Clinical findings

Clinical, EEG and MRI findings observed in the four patients are summarized in Table 1 and presented in detail in the Supplementary material. In brief, early manifestations, observed in all patients, were developmental delay and febrile seizures, evolving in two patients to encephalopathy with profound delay, hypotonic/dyskinetic quadriparesis, intractable multiple seizure types and severe diffuse epileptiform EEG abnormalities (Patients 1 and 4) and to moderate delay with milder epilepsy and focal/multifocal EEG abnormalities in the other two (Patients 2 and 3).

Structural consideration of the v-ATPase mutations

We mapped the mutation sites of human ATP6V1A onto the crystal structure of the V_1 domain from a prokaryotic homologue, *E. hirae* v-ATPase, in a nucleotide-bound state (PDB code 3VR6) (Arai *et al.*, 2013). All the identified mutations fall into the A subunit of the V_1 domain (Fig. 2A).

Pro12 (Pro27 in human ATP6V1A) resides in the type I β-turn that is a part of the interaction interface between subunits A and B. Since the substitution of a proline residue with an arginine residue affects the main-chain conformation of the β-turn, the mutation may perturb the A–B interaction (Fig. 2A and B).

Asp85 (Asp100 in human ATP6V1A) makes a hydrogen bond with Arg89, a guanidium group that makes van der Waals contacts with adjacent hydrophobic side chains (Fig. 2B). As a result, the side chain of Asp85 is closely surrounded by hydrophobic residues, and its replacement with a bulkier tyrosine residue quite likely causes steric hindrance and destabilizes the protein folding. This is

supported by the FoldX calculation, which predicted a significant increase in free energy (about 13 kcal/mol) upon the Asp85Tyr mutation.

Asp329 (Asp349 in human ATP6V1A) is located near a nucleotide-binding site (Fig. 2B) and its side chain is involved in water-mediated coordination with a magnesium ion, which plays a critical role in the ATPase activity (Fig. 2B). Thus, the Asp329Asn mutation possibly impairs the catalytic function.

Asp351 (Asp371 in human ATP6V1A) is located at the interface among A, B and D subunits (Fig. 2A). The D subunit rotates within the A3B3 core along with the ATP hydrolysis, and thus the rotation process may be affected by the Asp351Gly mutation. The mutation sites were also mapped on the cryo-EM structure of the human homologue v-ATPase from the eukaryotic *S. cerevisiae* (rotational state 1, PDB code 3J9T) (Zhao *et al.*, 2015). As shown in Fig. 2B, the mapped mutation sites in the *S. cerevisiae* structure overlap with those of the *E. hirae*, suggesting that the predicted impact of the mutations on the prokaryotic structure is also valid for the eukaryotic orthologues.

Finally, we generated a homology model of human ATP6V1A (Supplementary Fig. 1) using *S. cerevisiae* A subunit as template, obtaining a high-confidence result (C-score 88% and TM-score 87%). The resulting structure shows a fold similar to the template (*cf.* Supplementary Fig. 1 and 2B), and the mutation sites are in the same locations of the *E. hirae* and *S. cerevisiae* structures.

Effects of *ATP6V1A* mutations on protein expression and stability

We addressed the impact of p.Asp349Asn and p.Asp100Tyr mutations on the ATP6V1A expression and stability by analysing HEK cells overexpressing ATP6V1A. Cells were transfected with vectors driving the expression of the wild-type or mutant variants in association with a Cherry fluorescent tag for identification. Immunocytochemistry of transfected cells coupled with quantitative western blot analysis showed a decreased expression of both ATP6V1A mutants that reached significance only for the

Table 1 Summary of clinical features in four patients carrying *ATP6V1A* mutations

	Patient			
	1	2	3	4
Origin/sex	Caucasian/F	Asian/M	Caucasian/F	Latino/M
Age at follow-up	14 years	8 years	8 years	11 years
ATP6V1A mutation	c.298G>T (p.Asp100Tyr) de novo	c.1045G>A (p.Asp349Asn) de novo	c.1112A>G (p.Asp371Gly) de novo	c.80C>G (p.Pro27Arg) de novo
Clinical diagnosis	Infantile onset epileptic encephalopathy	ID/epilepsy	ID/epilepsy	Infantile onset epileptic encephalopathy
Head circumference	At birth: 32 cm = 3rd %ile (−1.9 SD); at 12 years: 44.5 cm ⩽ 1st %ile (−7 SD): microcephaly	At birth: 33 cm = 10th %ile (−1.2 SD)	Unknown	At 12 months: 43.5 cm = 1st %ile (−2.2 SD); at 11 years: 49 cm ⩽ 1st %ile (−3.2 SD): microcephaly
Age/symptoms at first clinical presentation	11 months, hypotonia, developmental delay, seizures	1 month, developmental delay, jerky movement	2 years 6 months, developmental delay, seizures	7 months, hypotonia, developmental delay
Epilepsy	+	+	+	+
Age at seizure onset	11 months	2 years 10 months	2 years 6 months	11 months
Seizures types	Convulsive seizures during fever at onset, then infantile spasms, tonic, focal clonic, focal occipital	Convulsive seizures during fever at onset, then focal occipital	Convulsive seizures during fever at onset, then generalized tonic-clonic	Convulsive seizures during fever at onset, then spasms, tonic, clonic and myoclonic
Interictal EEG	Slow background, diffuse and multifocal epileptiform discharges	Posteriorly dominant, multifocal epileptiform discharges	Anteriorly predominant multifocal epileptiform discharges	Slow background, diffuse and multifocal epileptiform discharges
Brain MRI	Hypomyelination, mild brain and cerebellar atrophy	Normal at 7 years	Normal at 7 years	Mild atrophy at 1 years 5 months and 3 years 7 months
Clinical phenotype at last follow-up	Profound delay, non-verbal, no visual fixation, hypotonic/dyskinetic quadriparesis, non-ambulatory, early puberty (9 years).	Moderate ID (FSDQ: 53), poor language, headache, amelogenesis imperfecta diagnosed at 3 years, optic atrophy	Moderate ID, poor language, mild dysmorphic features (wide forehead, deep set eyes, beaked nose), behavioural abnormalities with autistic traits, wide based gait, hypotonia	Profound delay, non-verbal, no visual fixation, coloboma of the iris, hypotonic/dyskinetic quadriparesis, non-ambulatory

F = female; FSDQ = full scale developmental quotient; ID = intellectual disability; M = male; N/A = not available.
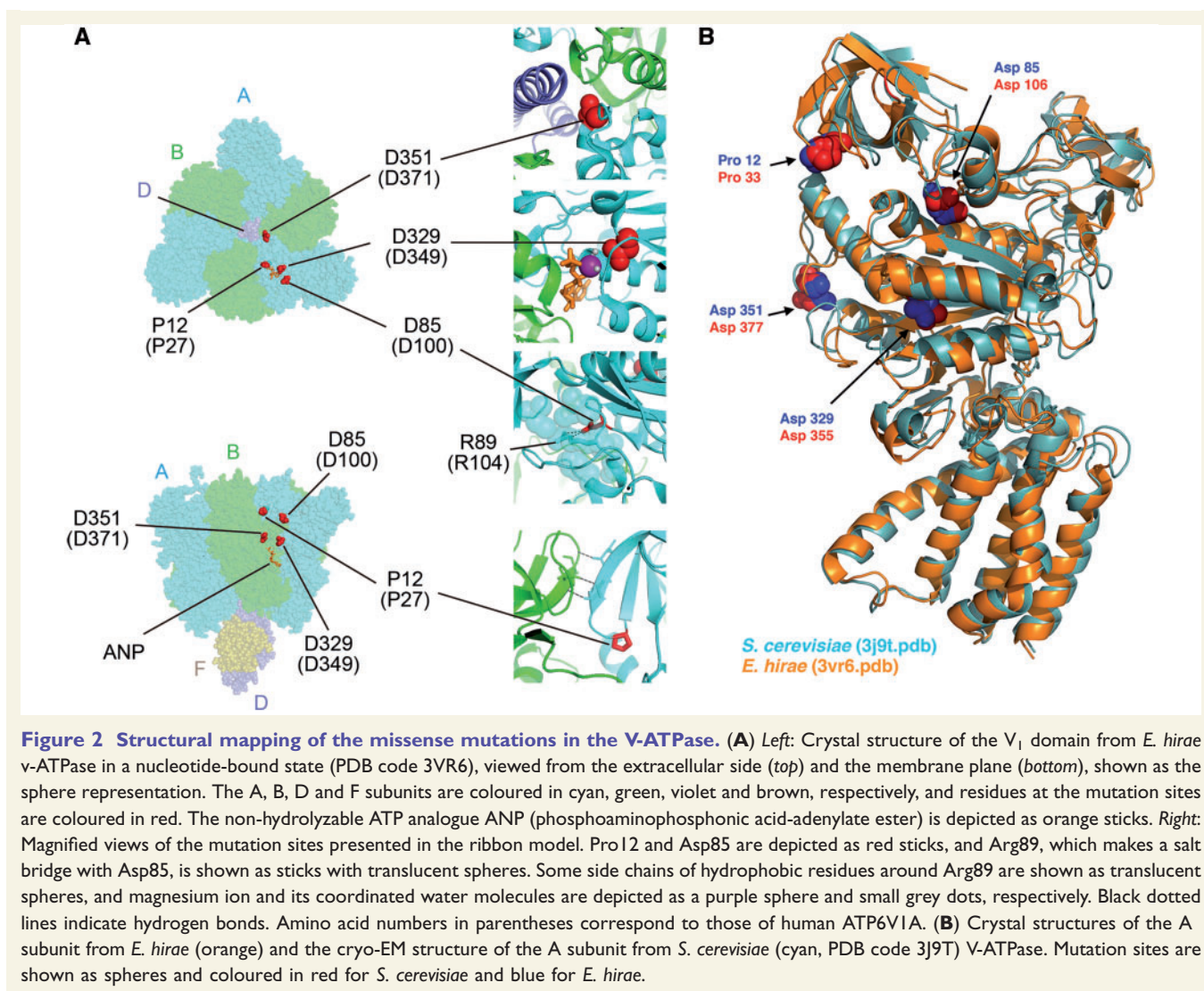
p.Asp100Tyr variant, and no overt subcellular mislocalization of both p.Asp100Tyr and p.Asp349Asn mutants with respect to wild-type ATP6V1A (Fig. 3A and B). The expression of the molecular partner, ATP6V1B2, was not modified either by p.Asp100Tyr or p.Asp349Asn mutation (Fig. 3B). To investigate the stability of ATP6V1A protein, we performed a degradation assay by treating transfected HEK cells with the protein synthesis inhibitor cycloheximide for various times. Compared to the wild-type isoform, both mutant ATP6V1A isoforms were less stable, although degradation was significantly increased only for the p.Asp100Tyr variant (Fig. 3C).

We next asked whether these findings could also be observed in patients' cells. To this end, we analysed the expression of endogenous ATP6V1A protein in patients' lymphoblasts and compared it with the respective healthy parents' cells (Fig. 3D and E). While the expression of ATP6V1A and ATP6V1B2 was not modified in Asp349Asn proband's cells with respect to his healthy mother's cells, a significant decrease of ATP6V1A, but not ATP6V1B2, expression was observed in Asp100Tyr proband's cells. These data are in full agreement with the structural analysis prediction of a folding defect in the p.Asp100Tyr mutant (Fig. 2A) that may enhance its degradation.

ATP6V1A mutations result in lysosomal abnormalities

To examine the impact of the p.Asp349Asn and p.Asp100Tyr mutations in the regulation of pH homeostasis, we used the LysoTracker® probe to qualitatively evaluate intracellular acidic organelles in HEK cells overexpressing either pathogenic or wild-type ATP6V1A variants. Interestingly, the p.Asp349Asn mutant increased, while the p.Asp100Tyr mutant decreased, LysoTracker® fluorescence intensity (Fig. 4A). The LysoTracker® signal monitors both the actual pH of acidic organelles, namely endosomal and lysosomal compartments, and their relative abundance within the cell. Thus, we analysed in parallel the expression of the endosomal and lysosomal markers, EEA1 and LAMP1, respectively. Whereas EEA1 expression was unaltered in HEK cells expressing wild-type ATP6V1A or either pathogenic variants, the p.Asp100Tyr mutant was associated with a significant decrease of LAMP1 expression

Figure 2 Structural mapping of the missense mutations in the V-ATPase. (A) *Left*: Crystal structure of the V$_1$ domain from *E. hirae* v-ATPase in a nucleotide-bound state (PDB code 3VR6), viewed from the extracellular side (*top*) and the membrane plane (*bottom*), shown as the sphere representation. The A, B, D and F subunits are coloured in cyan, green, violet and brown, respectively, and residues at the mutation sites are coloured in red. The non-hydrolyzable ATP analogue ANP (phosphoaminophosphonic acid-adenylate ester) is depicted as orange sticks. *Right*: Magnified views of the mutation sites presented in the ribbon model. Pro12 and Asp85 are depicted as red sticks, and Arg89, which makes a salt bridge with Asp85, is shown as sticks with translucent spheres. Some side chains of hydrophobic residues around Arg89 are shown as translucent spheres, and magnesium ion and its coordinated water molecules are depicted as a purple sphere and small grey dots, respectively. Black dotted lines indicate hydrogen bonds. Amino acid numbers in parentheses correspond to those of human ATP6V1A. **(B)** Crystal structures of the A subunit from *E. hirae* (orange) and the cryo-EM structure of the A subunit from *S. cerevisiae* (cyan, PDB code 3J9T) V-ATPase. Mutation sites are shown as spheres and coloured in red for *S. cerevisiae* and blue for *E. hirae*.

evaluated by both single cell immunocytochemistry (Fig. 4B) and western blotting (Supplementary Fig. 2A). The data suggest that the p.Asp349Asn mutant exacerbates the acidic pH of intracellular organelles, while the p.Asp100Tyr mutant leads to a decreased expression of LAMP1-positive lysosomal structures. Lysosomes fuse with phagosomal and autophagosomal structures to generate autolysosomes and v-ATPase also acidifies autolysosomal organelles. We therefore investigated whether pathogenic *ATP6V1A* variants affect v-ATPase translocation to LC3-positive phagosomal structures. To this aim, we measured the co-localization between the v-ATPase subunit ATP6V1B2 and LC3 in HEK cells expressing wild-type ATP6V1A or either pathogenic variant. Both p.Asp100Tyr and p.Asp349Asn resulted in a decreased co-localization coefficient with respect to wild-type ATP6V1A (Fig. 4C). However, the v-ATPase translocation induced by cell starvation was slightly impaired by p.Asp100Tyr and substantially unaffected by p.Asp349Asn (Fig. 4C). No significant changes in LC3II/LC3I ratio and p62 accumulation were

observed in both experimental groups (Supplementary Fig. 2B). These data suggest a significant impact of both mutations on the recruitment of the v-ATPase to LC3-positive autolysosomal structures, with slightly impaired autophagic flux only for Asp100Tyr.

To verify whether altered lysosomal pH and levels of lysosomal markers were also present in patients, we subjected patients' lymphoblasts to the same analysis. Experiments using the ratiometric pH probe LysoSensor™ Yellow/Blue dextran, revealed a significant reduction in endocytic organelle pH in the Asp349Asn patient's lymphoblasts when compared to his healthy mother's lymphoblasts, in the absence of any change in the expression of LAMP1 and EEA1 (Fig. 5). Conversely, while the pH of endocytic organelles was not modified in the Asp100Tyr patient's lymphoblasts, a significant reduction in LAMP1 expression was observed (Fig. 5). Taken together, these data suggest a gain-of-function effect for the p.Asp349Asn mutation, characterized by an increased proton pumping into intracellular organelles, and a loss-of-function effect for the
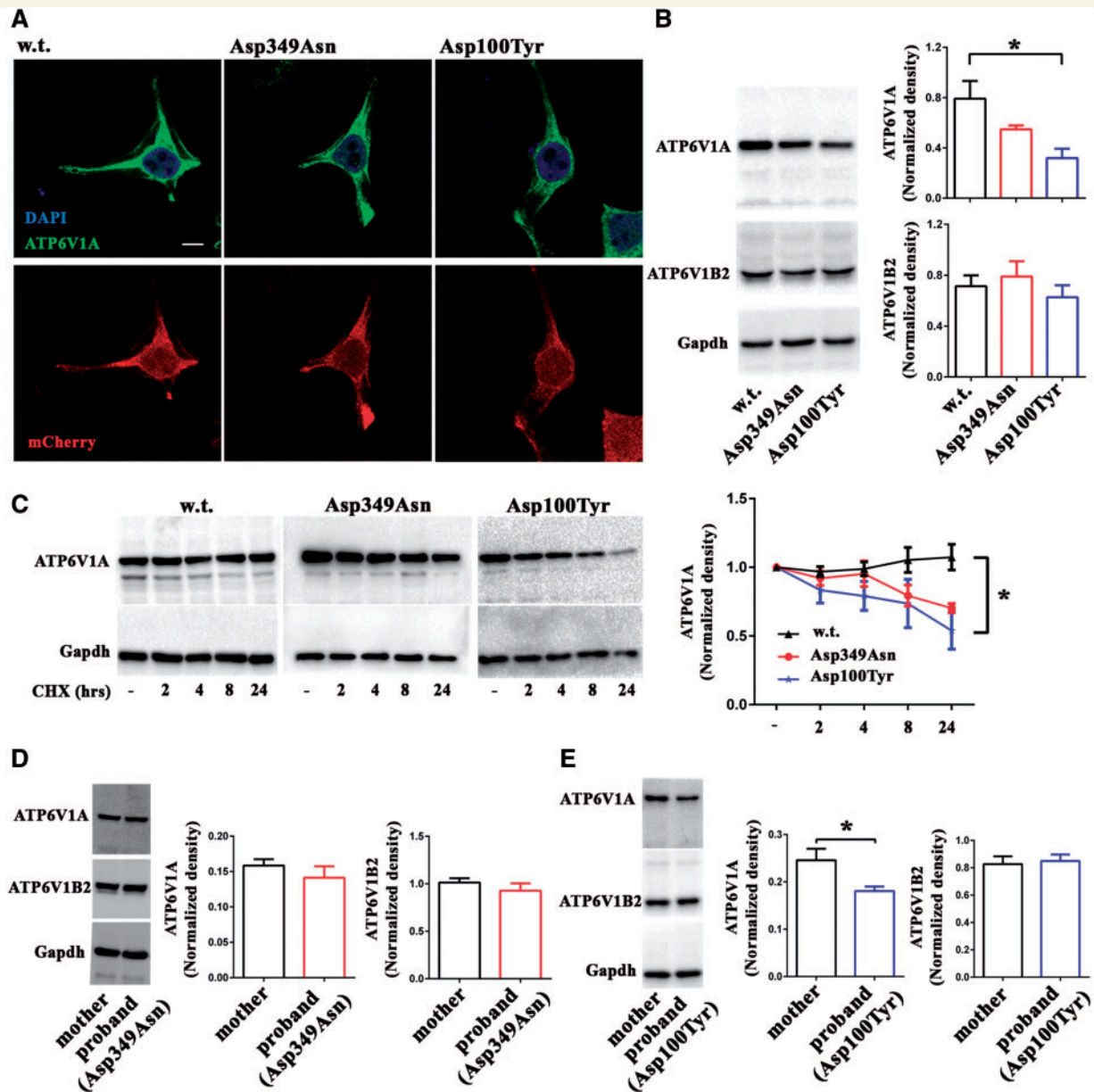
Figure 3 Impact of *ATP6V1A* mutations on protein expression and stability. (**A**) Representative images of HEK cells transfected with vectors coding wild-type ATP6V1A (w.t.), Asp349Asn ATP6V1A (Asp349Asn) or Asp100Tyr ATP6V1A (Asp100Tyr) variants. ATP6V1A immunolabelling, DAPI nuclear stain and Cherry reporter fluorescence are shown. Scale bar = 10 μm. (**B**) Representative western blot (*left*) from HEK cells transfected as above and lysed 24 h after transfection. ATP6V1A and ATP6V1B2 intensities were quantified by densitometric analysis with respect to GAPDH intensity (*right*). Data are means ± standard error of the mean (SEM) from five independent experiments. *$P < 0.05$ versus wild-type; Kruskall-Wallis/Dunn's tests. (**C**) *Left*: Representative western blots of HEK cell lysates stained with anti-ATP6V1A antibody and anti-GADPH as loading control. Cells were transfected with wild-type, Asp349Asn or Asp100Tyr ATP6V1A variants and incubated with cycloheximide for 2, 4, 8, 24 h or vehicle (DMSO; 24 h) as a control (–). *Right*: Densitometric analysis of ATP6V1A intensity with respect to GADPH expressed in percent of control samples without cycloheximide. Data are means ± SEM from four independent experiments. The areas under the respective curves were compared using the Kruskal-Wallis/Dunn's tests. *$P < 0.05$ versus wild-type. (**D**) Representative western blot from lymphoblast lysates (30 μg) of patient affected by the Asp349Asn mutation (proband) and the healthy mother. (**E**) Representative western blot from lymphoblast lysates (30 μg) of patient affected by the Asp100Tyr mutation (proband) and the healthy mother. In **D** and **E**, ATP6V1A and ATP6V1B2 intensity were quantified by densitometric analysis with respect to GADPH. Data are means ± SEM from four independent experiments. *$P < 0.05$; Mann Whitney U-test.
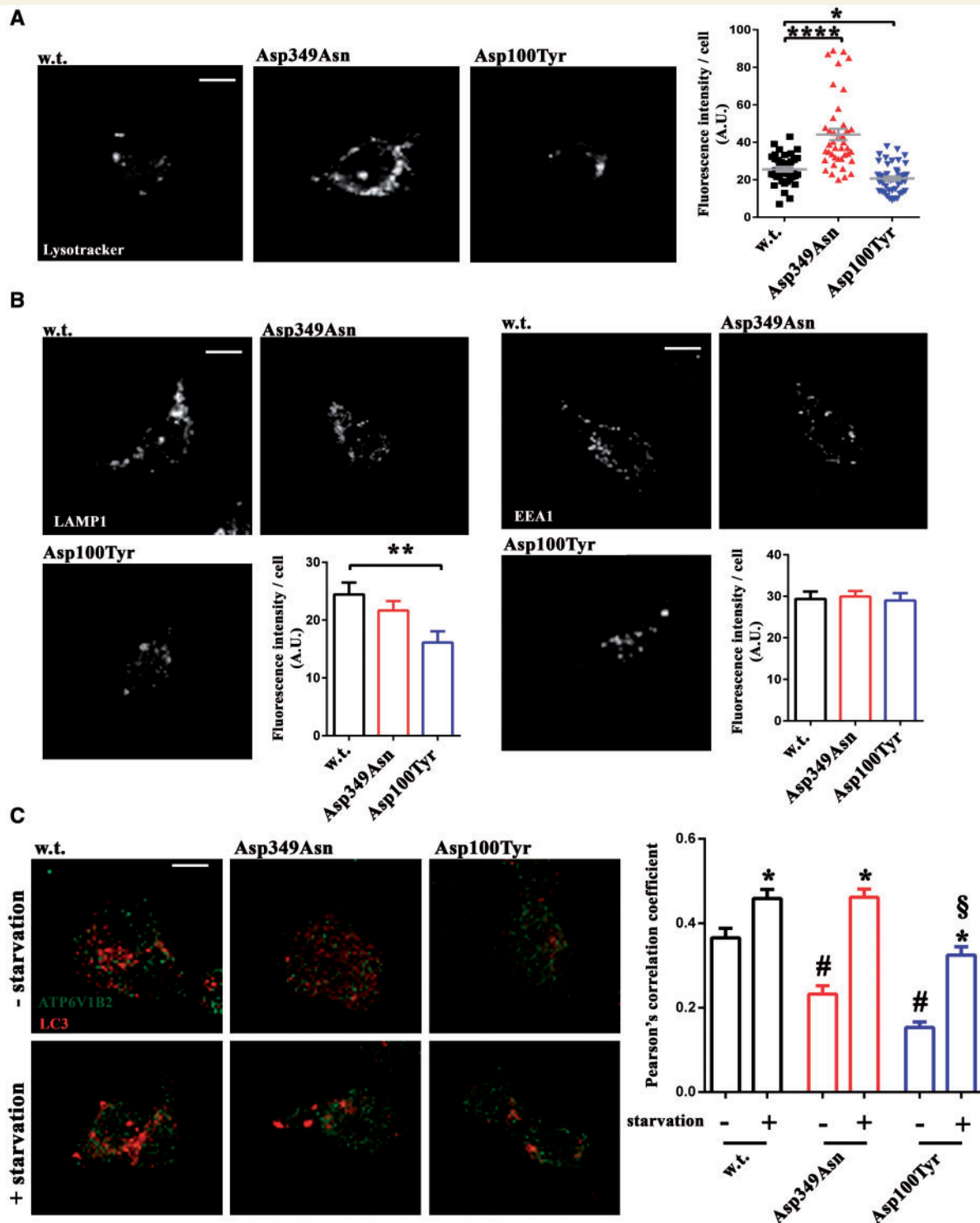
Figure 4 Effects of *ATP6V1A* mutations on endo-lysosomal markers and v-ATPase recruitment to autophagosomes.
(**A**) *Left*: Representative images of HEK cells transfected with wild-type ATP6V1A (w.t.), Asp349Asn ATP6V1A (Asp349Asn) or Asp100Tyr ATP6V1A (Asp100Tyr) variants and incubated with LysoTracker® (200 nM, 1 h). *Right*: LysoTracker® fluorescence intensity was quantified in 38 (wild-type), 41 (Asp349Asn) and 45 (Asp100Tyr) cells from three independent experiments. Individual data and means ± SEM are shown. *$P < 0.05$, ****$P < 0.0001$ versus wild-type; Kruskall-Wallis/Dunn's tests. (**B**) Representative images and densitometric quantification from HEK cells transfected as above and immunolabelled with LAMP1 (*left*) or EEA1 (*right*). Histograms show quantification of signal intensity. Data are means ± SEM of 24–33 cells per experimental condition, from three independent experiments. **$P < 0.001$ versus wild-type Kruskall-Wallis/ Dunn's tests. (**C**) Representative images from HEK cells transfected as above and immunolabelled with ATP6V1B2 and LC3B under control conditions or after starvation for 2 h. Graph shows the quantification of ATP6V1B2 and LC3B co-localization using ImageJ software to determine the Pearson's correlation coefficient. Data are means ± SEM of 30 cells per experimental condition. *$P < 0.05$ versus respective control; #$P < 0.001$ versus non-starved wild-type; §$P < 0.001$ versus starved wild-type. Data were analysed by two-way ANOVA/Bonferroni's tests.
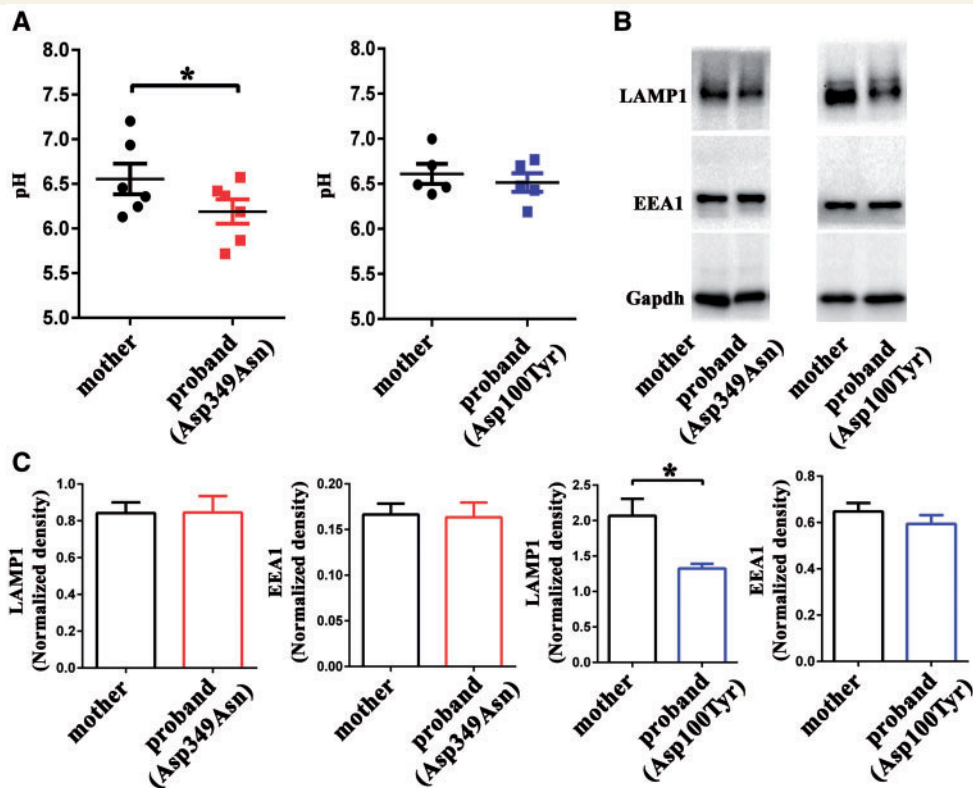
Figure 5 Effects of *ATP6V1A* mutations on intracellular organelle pH and endo-lysosomal markers in patients' cells.
(**A**) Quantification of endocytic organelle pH in lymphoblasts from patients (probands) bearing either p.Asp349Asn (red) or p.Asp100Tyr (blue) mutation and the respective healthy mothers (black). Individual data and means ± SEM of five to six independent measurements are shown. *$P < 0.05$; Wilcoxon matched pairs signed rank test. (**B**) Representative western blot from lymphoblast lysates (30 µg) as defined above. LAMP1, EEA1 and GADPH as loading control is shown. (**C**) LAMP1 and EEA1 immunoreactivities were quantified by densitometric analysis and normalized to GADPH. Data are means ± SEM from four independent experiments. *$P < 0.05$; Mann-Whitney U-test.

p.Asp100Tyr mutation associated with defects in lysosomal compartments.

ATP6V1A mutations impact on neuronal pH homeostasis and neuronal development

In view of the neurodevelopmental phenotype observed in the four patients carrying *de novo* heterozygous *ATP6V1A* mutations, we investigated whether the effects on lysosomal homeostasis observed in HEK cells and patient-derived lymphoblasts were recapitulated in neurons. To address this question, we transiently expressed ATP6V1A and the pathogenic mutants thereof in rat hippocampal neuronal cultures and evaluated intracellular acidic organelles by LysoTracker® staining at the neuronal soma. As shown in Fig. 6A, neurons overexpressing p.Asp349Asn resulted in a significantly higher LysoTracker® staining as compared to wild-type ATP6V1A-expressing neurons. In contrast, p.Asp100Tyr ATP6V1A overexpression induced a significant loss of LysoTracker® staining. Thus, the expression of the two mutants in neurons precisely phenocopies the

effects observed in cell lines, suggesting that such an alteration in pH and lysosomal homeostasis also occurs in brain cells.

To investigate cellular correlates of the patients' neurodevelopmental delay and explore whether the defects in LysoTracker® signal have an impact on neuronal development, we transfected rat hippocampal neurons at 7 DIV and analysed neurite elongation at 10 DIV by Sholl analysis. The analysis revealed a similar and significant loss of neurite arborization for both p.Asp349Asn- and p.Asp100Tyr-expressing neurons, indicating that both pathogenic variants significantly affect the outgrowth and branching of neuronal processes during development (Fig. 6B).

ATP6V1A mutations affect synapse formation in primary neurons

In developing neurons, neurite elongation is followed by synapse formation and stabilization. V-ATPase is a fundamental protein component of synaptic vesicles, where it allows neurotransmitter loading and regulates synaptic
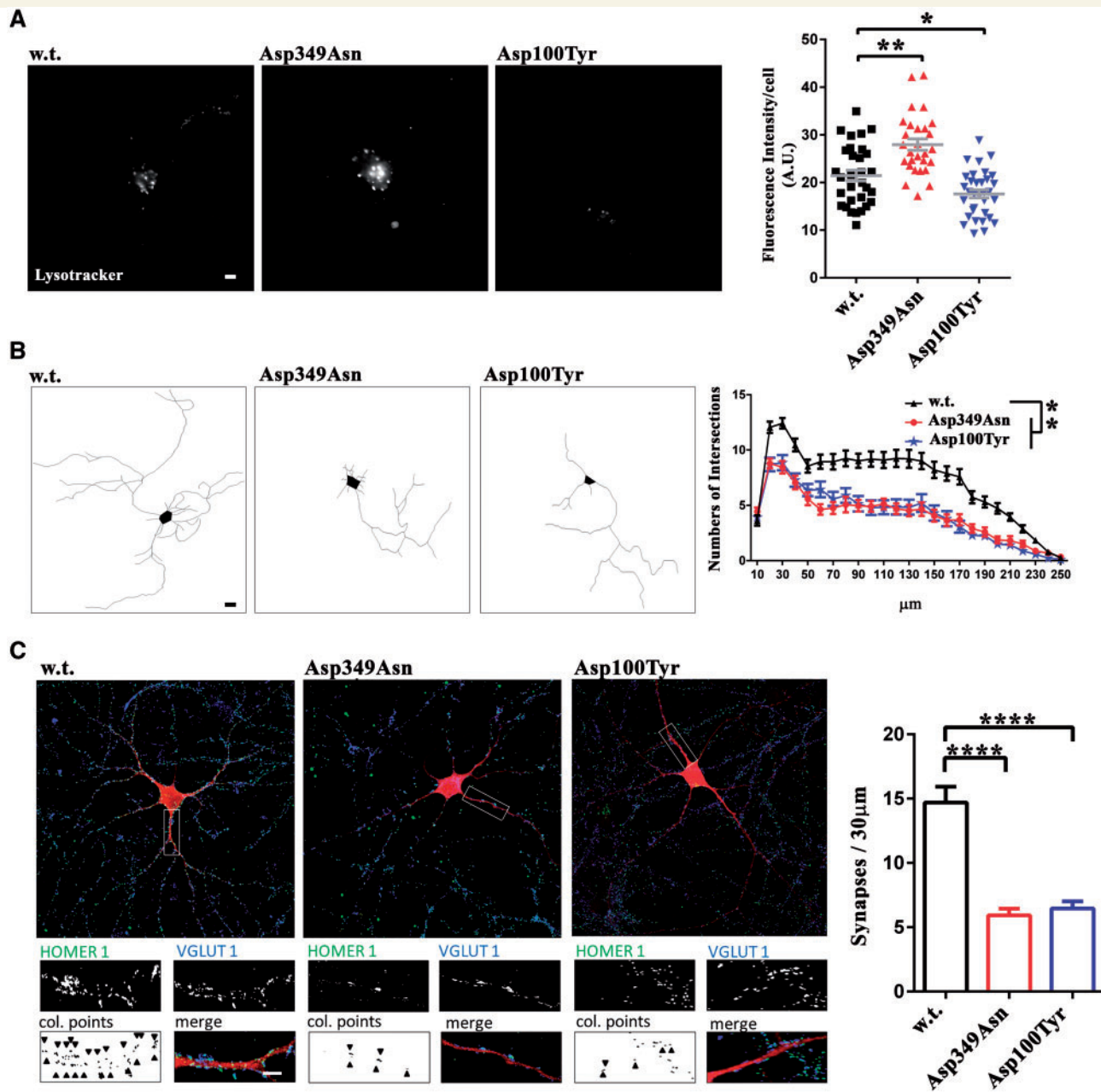
Figure 6 Effect of *ATP6V1A* mutations on pH homeostasis, development and synaptic connectivity in primary hippocampal neurons. (**A**) *Left*: Representative images of rat hippocampal neurons transfected with wild-type (w.t.), Asp349Asn (Asp349Asn) and Asp100Tyr (Asp100Tyr) ATP6V1A variants at 7 DIV and incubated with LysoTracker® (50 nM, 30 min) at 10 DIV. *Right*: LysoTracker® fluorescence intensity was quantified in 31 (wild-type), 28 (Asp349Asn) and 33 (Asp100Tyr) neurons from two independent preparations. Individual data and means ± SEM are shown. *$P < 0.05$, **$P < 0.01$ versus wild-type; Kruskall-Wallis/Dunn's tests. (**B**) *Left*: Representative neurite traces of 10 DIV neurons transfected as in **A**. *Right*: Sholl analysis of neurite arborization as a function of distance from the soma. Data are means ± SEM of 29–33 neurons for experimental group from three independent preparations. **$P < 0.01$ versus wild-type; Kruskall-Wallis/Dunn's tests. (**C**) *Left*: Representative images of hippocampal neurons transfected with wild-type ATP6V1A (w.t.), Asp349Asn ATP6V1A (Asp349Asn) or Asp100Tyr ATP6V1A (Asp100Tyr) variants (*top*) at 14 DIV and analysed at 17 DIV. White rectangles indicate proximal dendrites shown at high magnification (*bottom*). Synaptic boutons were identified by double immunostaining for VGLUT1 (blue) and Homer1 (green). The co-localization panels (col. points) highlight the double-positive puncta (black), marked by arrowheads, corresponding to *bona fide* synapses. The merge panels show positive puncta along transfected branches. Scale bar = 10 μm. *Right*: Quantitative analysis of synaptic puncta counted on 30-μm branches starting from the cell body. Data are means ± SEM of 27–28 neurons per experimental condition, from three independent preparations. ****$P < 0.0001$ versus wild-type; two-way ANOVA/Bonferroni's tests.

transmission (Takamori *et al.*, 2006; Takamori, 2016). Moreover, acidic lysosomes have been recently described at excitatory postsynaptic sites (Goo *et al.*, 2017; Padamsey *et al.*, 2017). Accordingly, the expression of the v-ATPase V_1 subunits, ATP6V1A and ATP6V1B2, was found to increase with *in vitro* neuronal maturation and synaptogenesis along with the expression of pre- and postsynaptic markers (Supplementary Fig. 3A).

To study the effects of ATP6V1A mutants on synapse formation, we transfected hippocampal neurons at 14 DIV and analysed synapse density at 17 DIV. Excitatory synaptic contacts were visualized by double immunostaining with the presynaptic marker VGLUT1 and the postsynaptic marker Homer1 to identify mature excitatory synapses unambiguously. Synapse counting at 30 μm distance from the cell body revealed a significant loss of excitatory synaptic connections for p.Asp349Asn and p.Asp100Tyr overexpressing neurons, suggesting that both pathogenic variants dramatically impair the formation and maintenance of excitatory synapses (Fig. 6C). Similar effects on the density of excitatory synaptic contacts were observed after treatment of hippocampal neurons with the lysosomal enzyme inhibitor leupeptin (Supplementary Fig. 3B).

Discussion

The phenotypic features observed in the four patients reported here can be typically described as developmental encephalopathy with epilepsy and subsumed as *ATP6V1A* encephalopathy, although a larger number of observations is necessary to reveal the whole phenotypic spectrum. However, gathering a large series may take a long time because *ATP6V1A* mutations are very rare, and have not emerged before in large cohorts with epileptic and developmental encephalopathies (Allen *et al.*, 2013; Appenzeller *et al.*, 2014; McRae *et al.*, 2017); we could only identify four cases through whole exome sequencing studies on 1444 probands from three continents. Querying the denovo-db, we found only two potential *de novo* variants in the coding regions of *ATP6V1A*, thus further highlighting the rarity of *de novo* variants in this gene. Pathogenicity of the *de novo* p.Pro27Arg, p.Asp100Tyr, p.Asp349Asn and p.Asp371Gly variants could be established based on their: (i) occurrence in four patients with a developmental encephalopathy with epilepsy, the genome-wide statistical significance for missense *de novo* mutations enrichment; (ii) absence from publicly available databases; (iii) causing substitutions at highly evolutionarily conserved amino acid positions; and (iv) predicted highly damaging consequences emerging from *in silico* methods and the high intolerance of the *ATP6V1A* gene to variations. Accordingly, structural modelling allowed to localize the mutated sites in regions of ATP6V1A responsible for either the proper folding of the subunit (p.Asp100Tyr), the interaction with the V_0 B

subunit (p.Pro27Arg) or the function of the v-ATPase complex (p.Asp349Asn, p.Asp371Gly).

As most causative variations occur with very low allele frequency within each gene and only account for a small fraction of epilepsy patients (Myers and Mefford, 2015) sequencing large cohorts of patients, collected through large networks and gene-matching tools has higher chances to find multiple affected individuals carrying *de novo* mutations in the same gene(s) (Hamdan *et al.*, 2017). This strategy can overcome the challenge to determine whether the candidate *de novo* mutations have a causal relationship with the disease or are found by chance. A statistical framework specifically developed to address this challenge (Samocha *et al.*, 2014), and successfully applied to developmental disorders in previous studies (Lelieveld *et al.*, 2016; McRae *et al.*, 2017), has also proved instrumental to demonstrate that *ATP6V1A* reached genome-wide statistical significance for missense *de novo* mutations enrichment in our cohort.

The Online Mendelian Inheritance in Man (OMIM) catalogue contains 59 entries for early infantile epileptic encephalopathies featuring intellectual disability and epilepsy (https://www.omim.org/entry/308350?search = EIEE&highlight = eiee) (Supplementary Table 3), caused by mutations in as many genes, and mentions that similar phenotypes are also observed in other genetic disorders, highlighting the extreme genetic heterogeneity underlying this category.

The many genes that have been associated with such complex developmental epilepsy conditions have revealed the pathogenic role of mutations affecting diverse molecular pathways that regulate ion channel functioning, membrane excitability, synaptic plasticity, neurotransmitter release, postsynaptic receptors, transporters, cell metabolism, and many formative steps in early brain development such as the proliferation and migration of neuronal precursors, dendritogenesis, synaptogenesis, cell and glial biology (Guerrini and Noebels, 2014). Our experimental work on the p.Asp100Tyr and p.Asp349Asn missense substitutions indicates that *ATP6V1A* mutations cause functional defects in v-ATPase physiology with alterations of lysosomal homeostasis associated with abnormal neuritogenesis and synaptic density.

The main function of v-ATPase is proton transport and acidification of intracellular organelles, in particular lysosomes that have critical requirements for pH. The functional experiments performed on the p.Asp100Tyr mutation, causing the more severe phenotype, demonstrated an increased degradation with impaired expression of ATP6V1A and lower lysosomal abundance. This finding was also associated with decreased recruitment of v-ATPase by autophagosomes under basal and starvation conditions, suggesting a potential impairment of the autophagic flux, as recently described in patients with mutations in the accessory v-ATPase subunit *ATP6AP2* (Rujano *et al.*, 2017). Conversely, p.Asp349Asn, which was associated with a milder phenotype, resulted in decreased endo-lysosomal pH, with no effects on either expression of the mutant

protein or lysosomal abundance, pointing to a gain-of-function effect. This variant slightly impairs v-ATPase translocation to autophagosomes under basal, but not starvation, conditions, suggesting that the formation of autolysosomes is preserved. These functional findings were supported by structural modelling results, predicting that the p.Asp100Tyr mutation decreases protein stability, whereas p.Asp349Asn affects the catalytic activity of v-ATPase.

When modelled in hippocampal neurons, these pathogenic mutations produced the same significant and divergent effects on lysosomal marker intensity and endolysosomal pH that were observed in cell lines and probands' lymphoblasts, reflecting their relevance for the CNS. Moreover, in primary neurons, both p.Asp100Tyr and p.Asp349Asn mutants induced significant and comparable defects in dendrite development and excitatory synapse formation. The neuronal phenotype of both mutants demonstrates a previously unexplored role of the v-ATPase in the processes of neuronal development and connectivity. Similarities in changes on synapse formation induced by the two tested mutations and by leupeptin, a known inhibitor of lysosomal function, suggest an important pathophysiological role of altered lysosomal homeostasis. This hypothesis is also supported by recent reports on novel roles of lysosomes at the synapse for the turnover of synaptic proteins, as well as for the plasticity of dendritic spines (Goo *et al.*, 2017; Padamsey *et al.*, 2017; Sambri *et al.*, 2017).

Although the precise molecular mechanisms through which the described *de novo* mutations result in a developmental encephalopathy with epilepsy remain to be clarified, we here propose that alteration in lysosomal homeostasis may represent a novel pathogenic mechanism for this aetiologically heterogeneous group of disorders. Further work is needed to clarify the role of v-ATPase in brain development and to precisely establish the cellular signalling pathways that can be altered by loss of lysosomal homeostasis.

It is often impossible to disentangle whether the developmental or epileptic component is more important in contributing to a patient's presentation. In the four patients described here, however, there was good correspondence between severity of epilepsy and overall neurodevelopmental impairment, which might suggest either a more severe brain dysfunction leading to both severe impairment and to the epileptic encephalopathy or a deleterious effect of early severe and long-lasting epilepsy on development.

Next generation sequencing studies have demonstrated that sporadic developmental disorders associated with epilepsy, once considered potentially recessive in nature, often arise from *de novo* mutations of dominant genes and that the same gene can be associated with a broader phenotypic spectrum than originally believed (Mei *et al.*, 2017). Our findings clearly link the *ATP6V1A* gene with a dominant form of encephalopathy after two biallelic homozygous missense mutations of the same gene had been related in three individuals to cutis laxa, a rare, severe systemic disorder, leading to early death in one of the patients and featuring, in addition to generalized skin wrinkling, marked hypotonia, dysmorphic facial features, cardiac abnormalities, structural brain abnormalities and seizures (Van Damme *et al.*, 2017). Although comparison between our patients and the three previously reported with biallelic *ATP6V1A* mutations is only partially feasible, there is evidence that biallelic mutations cause a more complex phenotype in which severe neurological manifestations are part of a multi-organ involvement. A number of additional genetic developmental disorders with epilepsy, including those related to *PRRT2* (Ebrahimi-Fakhari *et al.*, 2015), *TBC1D24* (Balestrini *et al.*, 2016), *RELN* (Dazzo *et al.*, 2015) and *SLC2A1* (Wang *et al.*, 2000) genes, have been associated with both autosomal dominant and more severe recessive phenotypes.

Supplementary material

Supplementary material is available at *Brain* online.

References

Allen AS, Berkovic SF, Cossette P, Delanty N, Dlugos D, Eichler EE, et al. *De novo* mutations in epileptic encephalopathies. Nature 2013; 501: 217–21.

Appenzeller S, Balling R, Barisic N, Baulac S, Caglayan H, Craiu D, et al. *De novo* mutations in synaptic transmission genes including DNM1 cause epileptic encephalopathies. Am J Hum Genet 2014; 95: 360–70.

Arai, S, Saijo S, Suzuki K, Mizutani K, Kakinuma Y, Ishizuka-Katsura Y, et al. Rotation mechanism of *Enterococcus hirae* V1-ATPase based on asymmetric crystal structures. Nature 2013; 493: 703–77.

Balestrini S, Milh M, Castiglioni C, Lüthy K, Finelli MJ, Verstreken P, et al. TBC1D24 genotype-phenotype correlation: epilepsies and other neurologic features. Neurology 2016; 87: 77–85.

Bodzęta A, Kahms M, Klingauf J. The presynaptic v-ATPase reversibly disassembles and thereby modulates exocytosis but is not part of the fusion machinery. Cell Rep 2017; 20: 1348–59.

Cingolani P, Platts A, Wang le L, Coon M, Nguyen T, Wang L, et al. Program for annotating and predicting the effects of single nucleotide polymorphisms, SnpEff: SNPs in the genome of Drosophila melanogaster strain w1118; iso-2; iso-3. Fly 2012; 6: 80–92.

Cotter K, Stransky L, McGuire C, Forgac M. Recent insights into the structure, regulation, and function of the v-ATPases. Trends Biochem Sci 2015; 40: 611–22.

Dazzo E, Fanciulli M, Serioli E, Minervini G, Pulitano P, Binelli S, et al. Heterozygous reelin mutations cause autosomal-dominant lateral temporal epilepsy. Am J Hum Genet 2015; 96: 992–1000.

DePristo MA, Banks E, Poplin R, Garimella KV, Maguire JR, Hartl C, et al. A framework for variation discovery and genotyping using next-generation DNA sequencing data. Nat Genet 2011; 43: 491–8.

Ebrahimi-Fakhari D, Saffari A, Westenberger A, Klein C. The evolving spectrum of PRRT2-associated paroxysmal diseases. Brain 2015; 138: 3476–95.

Falace A, Filipello F, La Padula V, Vanni N, Madia F, De Pietri Tonelli D, et al. TBC1D24, an ARF6-interacting protein, is mutated in familial infantile myoclonic epilepsy. Am J Hum Genet 2010; 87: 365–70.

Fischer B, Dimopoulou A, Egerer J, Gardeitchik T, Kidd A, Jost D, et al. Further characterization of ATP6V0A2-related autosomal recessive *cutis laxa*. Hum Genet 2012; 131: 1761–73.

Forgac M. Vacuolar ATPases: rotary proton pumps in physiology and pathophysiology. Nat Rev Mol Cell Biol 2007; 11: 917–29.

Frattini A, Orchard PJ, Sobacchi C, Giliani S, Abinun M, Mattsson JP, et al. Defects in TCIRG1 subunit of the vacuolar proton pump are responsible for a subset of human autosomal recessive osteopetrosis. Nat Genet 2000; 25: 343–6.

Goo MS, Sancho L, Slepak N, Boassa D, Deerinck TJ, Ellisman MH, et al. Activity-dependent trafficking of lysosomes in dendrites and dendritic spines. J Cell Biol 2017; 216: 2499–513.

Guerrini R, Noebels J. How can advances in epilepsy genetics lead to better treatments and cures? Adv Exp Med Biol 2014; 813: 309–17.

Hamdan FF, Myers CT, Cossette P, Lemay P, Spiegelman D, Laporte AD, et al. High rate of recurrent *de novo* mutations in developmental and epileptic encephalopathies. Am J Hum Genet 2017; 101: 664–85.

Ioannidis NM, Rothstein JH, Pejaver V, Middha S, McDonnell SK, Baheti S, et al. REVEL: an ensemble method for predicting the pathogenicity of rare missense variants. Am J Hum Genet 2016; 99: 877–85.

Ionita-Laza I, McCallum K, Xu B, Buxbaum JD. A spectral approach integrating functional genomic annotations for coding and noncoding variants. Nat Genet 2016; 48: 214–20.

Iossifov I, O'Roak BJ, Sanders SJ, Ronemus M, Krumm N, Levy D, et al. The contribution of *de novo* coding mutations to autism spectrum disorder. Nature 2014; 515: 216–21.

Itan Y, Shang L, Boisson B, Ciancanelli MJ, Markle JG, Martinez-Barricarte R, et al. The mutation significance cutoff: gene-level thresholds for variant predictions. Nat Methods 2016; 13: 109–10.

Itan Y, Shang L, Boisson B, Patin E, Bolze A, Moncada-Vélez M, et al. The human gene damage index as a gene-level approach to prioritizing exome variants. Proc Natl Acad Sci USA 2015; 112: 13615–20.

Jagadeesh KA, Wenger AM, Berger MJ, Guturu H, Stenson PD, Cooper DN, et al. M-CAP eliminates a majority of variants of uncertain significance in clinical exomes at high sensitivity. Nat Genet 2016; 48: 1581–6.

Karet FE, Finberg KE, Nelson RD, Nayir A, Mocan H, Sanjad SA, et al. Mutations in the gene encoding B1 subunit of H+-ATPase cause renal tubular acidosis with sensorineural deafness. Nat Genet 1999; 21: 84–90.

Kelley LA, Mezulis S, Yates CM, Wass MN, Sternberg MJ. The Phyre2 web portal for protein modeling, prediction and analysis. Nat Protoc 2015; 10: 845–58.

Kircher M, Witten DM, Jain P, O'Roak BJ, Cooper GM, Shendure J. A general framework for estimating the relative pathogenicity of human genetic variants. Nat Genet 2014; 46: 310–15.

Kornak U, Reynders E, Dimopoulou A, van Reeuwijk J, Fischer B, Rajab A, et al. Impaired glycosylation and cutis laxa caused by mutations in the vesicular H(+)-ATPase subunit ATP6V0A2. Nat Genet 2008; 40: 32–4.

Kornak U, Schulz A, Friedrich W, Uhlhaas S, Kremens B, Voit T, et al. Mutations in the a3 subunit of the vacuolar H(+)-ATPase cause infantile malignant osteopetrosis. Hum Mol Genet 2000; 9: 2059–63.

Kortum F, Caputo V, Bauer CK, Stella L, Ciolfi A, Alawi M, et al. Mutations in KCNH1 and ATP6V1B2 cause Zimmermann-Laband syndrome. Nat Genet 2015; 47: 661–7.

Lek M, Karczewski KJ, Minikel EV, Samocha KE, Banks E, Fennell T, et al. Exome Aggregation Consortium. Analysis of protein-coding genetic variation in 60,706 humans. Nature 2016; 536: 285–91.

Lelieveld SH, Reijnders MR, Pfundt R, Yntema HG, Kamsteeg EJ, de Vries P, et al. Meta-analysis of 2,104 trios provides support for 10 new genes for intellectual disability. Nat Neurosci 2016; 19: 1194–6.

Li H, Durbin R. Fast and accurate long-read alignment with Burrows-Wheeler transform. Bioinformatics 2010; 26: 589–95.

Liu X, Wu C, Li C, Boerwinkle E. dbNSFP v3.0: a one-stop database of functional predictions and annotations for human nonsynonymous and splice-site SNVs. Hum Mutat 2016; 37: 235–41.

McKenna A, Hanna M, Banks E, Sivachenko A, Cibulskis K, Kernytsky A, et al. The genome analysis toolkit: a MapReduce framework for analyzing next-generation DNA sequencing data. Genome Res 2010; 20: 1297–303.

McRae JF, Clayton S, Fitzgerald TW, Kaplanis J, Prigmore E, Rajan D, et al. Prevalence and architecture of *de novo* mutations in developmental disorders. Nature 2017; 542: 433–8.

Mei D, Parrini E, Marini C, Guerrini R. The impact of next-generation sequencing on the diagnosis and treatment of epilepsy in paediatric patients. Mol Diagn Ther 2017; 21: 357–73.

Morel N, Poëa-Guyon S. The membrane domain of vacuolar H⁺ATPase: a crucial player in neurotransmitter exocytotic release. Cell Mol Life Sci 2015; 72: 2561–73.

Myers CT, Mefford HC. Advancing epilepsy genetics in the genomic era. Genome Med 2015; 7: 91.

Narayanan M, Ramsey K, Grebe T, Schrauwen I, Szelinger S, Huentelman M, et al. Case report: compound heterozygous nonsense mutations in TRMT10A are associated with microcephaly, delayed development, and periventricular white matter hyperintensities. F1000Res 2015; 4: 912.

Padamsey Z, McGuinness L, Bardo SJ, Reinhart M, Tong R, Hedegaard A, et al. Activity-dependent exocytosis of lysosomes regulates the structural plasticity of dendritic spines. Neuron 2017; 93: 132–46.

Petrovski S, Wang Q, Heinzen EL, Allen AS, Goldstein DB. Genic intolerance to functional variation and the interpretation of personal genomes. PLoS Genet 2013; 9: e1003709.

Ramu A, Noordam MJ, Schwartz RS, Wuster A, Hurles ME, Cartwright RA, et al. DeNovoGear: de novo indel and point mutation discovery and phasing. Nat Methods 2013; 10: 985–7.

Roy A, Kucukural A, Zhang Y. I-TASSER: a unified platform for automated protein structure and function prediction. Nat Protoc 2010; 5: 725–38.

Rujano MA, Cannata Serio M, Panasyuk G, Péanne R, Reunert J, Rymen D, et al. Mutations in the X-linked ATP6AP2 cause glycosilation disorder with autophagic defect. J Exp Med 2017; 214: 3707–29.

Saitsu H, Nishimura T, Muramatsu K, Kodera H, Kumada S, Sugai K, et al. De novo mutations in the autophagy gene WDR45 cause static encephalopathy of childhood with neurodegeneration in adulthood. Nat Genet 2013; 45: 445–9.

Sambri I, D'Alessio R, Ezhova Y, Giuliano T, Sorrentino NC, Cacace V, et al. Lysosomal dysfunction disrupts presynaptic maintenance and restoration of presynaptic function prevents neurodegeneration in lysosomal storage diseases. EMBO Mol Med 2017; 9: 112–32.

Samocha KE, Robinson EB, Sanders SJ, Stevens C, Sabo A, McGrath LM, et al. A framework for the interpretation of de novo mutation in human disease. Nat Genet 2014; 46: 944–50.

Smith AN, Skaug J, Choate KA, Nayir A, Bakkaloglu A, Ozen S, et al. Mutations in ATP6N1B, encoding a new kidney vacuolar proton pump 116-kD subunit, cause recessive distal renal tubular acidosis with preserved hearing. Nat Genet 2000; 26: 71–5.

Stover EH, Borthwick KJ, Bavalia C, Eady N, Fritz DM, Rungroj N, et al. Novel ATP6V1B1 and ATP6V0A4 mutations in autosomal recessive distal renal tubular acidosis with new evidence for hearing loss. J Med Genet 2002; 39: 796–803.

Takamori S. Presynaptic molecular determinants of quantal size. Front Synaptic Neurosci 2016; 8: 2.

Takamori S, Holt M, Stenius K, Lemke EA, Grønborg M, Riedel D. Molecular anatomy of a trafficking organelle. Cell 2006; 127: 831–46.

Turner TN, Yi Q, Krumm N, Huddleston J, Hoekzema K, Stessman HAF, et al. denovo-db: a compendium of human de novo variants. Nucleic Acids Res 2017; 45: D804–11.

Van Damme T, Gardeitchik T, Mohamed M, Guerrero-Castillo S, Freisinger P, Guillemyn B, et al. Mutations in ATP6V1E1 or ATP6V1A cause autosomal-recessive cutis laxa. Am J Hum Genet 2017; 100: 216–27.

Van der Auwera GA, Carneiro MO, Hartl C, Poplin R, Del Angel G, Levy-Moonshine A, et al. From FastQ data to high confidence variant calls: the genome analysis toolkit best practices pipeline. Curr Protoc Bioinformatics 2013; 43: 11.10.1–33.

Verstegen AM, Tagliatti E, Lignani G, Marte A, Stolero T, Atias M, et al. Phosphorylation of synapsin I by cyclin-dependent kinase-5 sets the ratio between the resting and recycling pools of synaptic vesicles at hippocampal synapses. J Neurosci 2014; 34: 7266–80.

Wang D, Kranz-Eble P, De Vivo DC. Mutational analysis of GLUT1 (SLC2A1) in Glut-1 deficiency syndrome. Hum Mutat 2000; 16: 224–31.

Ware JS, Samocha KE, Homsy J, Daly MJ. Interpreting de novo variation in human disease using denovolyzeR. Curr Protoc Hum Genet 2015; 87: 7.25.1–15.

Yuan Y, Zhang J, Chang Q, Zeng J, Xin F, Wang J, et al. De novo mutation in ATP6V1B2 impairs lysosome acidification and causes dominant deafness-onychodystrophy syndrome. Cell Res 2014; 24: 1370–3.

Zhao J, Benlekbir S, Rubinstein JL. Electron cryomicroscopy observation of rotational states in a eukaryotic v-ATPase. Nature 2015; 521: 241–5.